AEM
Journals.ASM.org

Nanoscale Structural and Mechanical Analysis of *Bacillus anthracis* Spores Inactivated with Rapid Dry Heating

Yun Xing,[a,b] Alex Li,[a] Daniel L. Felker,[c] Larry W. Burggraf[a]

Department of Engineering Physics, Air Force Institute of Technology, Wright-Patterson Air Force Base (WPAFB), Dayton, Ohio, USA[a]; Oak Ridge Institute for Science and Education (ORISE), Oak Ridge, Tennessee, USA[b]; Department of Systems Engineering & Management, Air Force Institute of Technology, WPAFB, Dayton, Ohio, USA[c]

Effective killing of *Bacillus anthracis* spores is of paramount importance to antibioterrorism, food safety, environmental protection, and the medical device industry. Thus, a deeper understanding of the mechanisms of spore resistance and inactivation is highly desired for developing new strategies or improving the known methods for spore destruction. Previous studies have shown that spore inactivation mechanisms differ considerably depending upon the killing agents, such as heat (wet heat, dry heat), UV, ionizing radiation, and chemicals. It is believed that wet heat kills spores by inactivating critical enzymes, while dry heat kills spores by damaging their DNA. Many studies have focused on the biochemical aspects of spore inactivation by dry heat; few have investigated structural damages and changes in spore mechanical properties. In this study, we have inactivated *Bacillus anthracis* spores with rapid dry heating and performed nanoscale topographical and mechanical analysis of inactivated spores using atomic force microscopy (AFM). Our results revealed significant changes in spore morphology and nanomechanical properties after heat inactivation. In addition, we also found that these changes were different under different heating conditions that produced similar inactivation probabilities (high temperature for short exposure time versus low temperature for long exposure time). We attributed the differences to the differential thermal and mechanical stresses in the spore. The buildup of internal thermal and mechanical stresses may become prominent only in ultrafast, high-temperature heat inactivation when the experimental timescale is too short for heat-generated vapor to efficiently escape from the spore. Our results thus provide direct, visual evidences of the importance of thermal stresses and heat and mass transfer to spore inactivation by very rapid dry heating.

Bacterial spores are metabolically dormant cells formed in a process called sporulation, which is generally induced by reduced levels of nutrients in the environment (1–3). Efficient inactivation of spores is of critical importance for a wide range of applications, including biodefense, food safety, environmental protection, and medical device sterilization (4–6). Spores are known to be more resistant to inactivation by heating, radiation exposure, and chemical decontamination than their corresponding vegetative cells. While various methods, including heating, chemical treatment, radiation, and UV treatment, have been used to inactivate spores (4, 6, 7), thermal inactivation is often the method of choice for many applications (8). Thermal inactivation of *Bacillus* spores in laboratory studies is most often achieved by wet heat in which spores are fully hydrated during heating (9–11) or dry heat in which dry spores are heated on a solid substrate, in an ampoule heated by an oil bath, in a hot air plume, or by infrared heating (5, 8, 12–20). It has long been observed that spores are much less resistant to heat in a well-hydrated environment than in a dry state (4). Moreover, the inactivation mechanisms are different under wet- and dry-heat conditions. It is known that wet-heat inactivation of wild-type *Bacillus subtilis* spores is associated with protein denaturation and enzyme inactivation (9, 11, 21), although specific damaged proteins that result in spore death remain to be identified. Spore killing by dry heat, on the other hand, is accompanied by the accumulation of DNA damage, including strand breaks initiated by depurination (14, 22, 23). These results come mainly from the biochemical and molecular biological analyses of inactivated and survivor spores. Damage to the spore structures and mechanical properties is relatively understudied, and their possible correlations to the biochemical results remain to be determined. A recent study by Tabit and Buys demonstrated by transmission electron microscopy that *Bacillus sporothermodurans* spores treated with wet heat at 130°C began to show structural damage to the cortical membrane after 4 min of heating and showed severe damage to the cortex and exosporium after 12 min of heating (10).

The spore's structure is considered to play important roles in spore resistance to various types of stresses, including ionizing radiation, reactive chemicals, UV photochemistry, and heat (4). Starting from the outside and proceeding inward, the spore layers include the loose-fitting exosporium (only for some spore-forming species, including *Bacillus anthracis*), the multilayered spore coats, the outer membrane, the peptidoglycan-rich cortex, the inner membrane, and the central core that contains most spore enzymes and spore nucleic acids (24). Analysis of spore architecture has mainly relied on electron microscopy (EM) techniques that frequently require sample preparation methods such as fixation, staining, dehydration, and embedding that may damage the native structural integrity of biological specimens (25). Nearly a decade ago, Plomp et al. (25) used atomic force microscopy (AFM) to directly visualize the native spore ultrastructure with unprecedented resolution. Since then, rapid progress has been made in applying AFM to study spore coat assembly, spore architecture, and germination dynamics (25–29). AFM images revealed previously unrecognized germination-induced alterations in spore

Received 22 October 2013 Accepted 21 December 2013
Published ahead of print 27 December 2013
Address correspondence to Yun Xing, yun.xing@afit.edu, or Alex Li., alex.li@afit.edu.

doi:10.1128/AEM.03483-13

coat architecture and in the disassembly of outer spore coat rodlet structures. These and other studies (30–39), including our previous work that showed that the spores of four closely related *Bacillus* species can be distinguished by AFM surface morphology analysis (37) have proved AFM to be a powerful tool complementary to EM techniques, providing three-dimensional images of native, minimally processed biological samples with nanometer resolution.

Originally invented for topographic imaging, AFM has evolved into a multifunctional molecular tool kit, enabling researchers not only to observe structural details of cells but also to measure the nanoscale chemical and physical properties of cells and the localization and properties of individual molecules (34, 40, 41). Using the AFM probe as a nanoindentation tool, AFM deflection data can be converted into load versus indentation depth plots and analyzed using theoretical models that provide quantitative information on the elasticity of the sample (represented by Young's modulus) (38, 39). More recently, cell hardness was found to correlate well with UV resistance and heat resistance, so Young's modulus measurement by AFM (or scanning probe method [SPM]) was proposed as a quick and direct method to determine resistance in some spore species (42). In summary, with its ability to observe single microbial cells at nanometer resolution, to monitor structural dynamics in response to environmental changes or chemicals, and to detect and manipulate single-cell surface constituents, AFM provides new insight into the structure-function relationships of cell envelopes and is having an increasingly important impact on many disciplines of microbiology, including cellular and molecular microbiology, pathogenesis, diagnosis, antimicrobial therapy, and environmental microbiology.

In this study, we have chosen *B. anthracis* spores to investigate rapid heat inactivation of bacterial spores because of their medical and military significance. *B. anthracis* is a Gram-positive, spore-forming bacterium that is the causative agent of the infectious disease anthrax. We have developed a rapid dry-heating system that allows us to quickly inactivate spores in a precisely controlled manner. We compared the inactivation efficiencies under various heating conditions and studied the structural alterations and nanomechanical properties of inactivated spores. This study compares the changes in nanoscale structural and mechanical properties of spores after rapid dry-heat inactivation.

MATERIALS AND METHODS

Bacterial strains and spore preparation. *Bacillus anthracis* Sterne strain (Thraxol-2, code 235-23) spores were grown on nutrient agar (Difco nutrient agar) for about 7 days at 35°C. Once phase-contrast microscopic examination confirmed spore purity (>95%), spores were harvested from the agar plates using a sterile cell scraper, then transferred to a sterile microcentrifuge tube, and finally washed five times with sterile deionized (DI) water. Clean spores were again confirmed by phase-contrast microscopy, suspended in DI water, and counted using a hemocytometer before the heat inactivation experiments started.

Rapid heat inactivation of *B. anthracis* Sterne spores. Heat inactivation of spores was achieved by using a conductive heating system designed in-house. This system generates a near-top hat heating profile for heating times as short as 0.1 s, which means that both the heating and cooling phases are considerably shorter than the steady-state heating phase; thus, the observed effects can be attributed mainly to the steady-state heating. Test samples were prepared using a drop of spore suspension containing 5.6×10^7 spores placed onto the surface of clean thin gold foil (60 μm thick) and left in a biosafety cabinet overnight to air dry. The spore-carrying pieces of gold foil were then folded and held closed using tweezers with ceramic tips. The use of ceramic-tipped tweezers minimized heat loss by conduction. The tweezer holding the gold foil was then mounted onto a computer-controlled translation stage. This motorized stage moved the sample rapidly into a preheated micro-oven for a set period of time and then quickly pulled it out. The temperature of the sample was monitored in real time using an infrared imaging system (FLIR infrared camera, model SC655).

Spore recovery from the substrate. Spores on the gold foil were recovered by a combined method of sonication and polyvinyl alcohol (PVA) stripping. The PVA method was adapted from a method reported by Moeller et al. (43). A droplet of 10% PVA solution was placed so that it would evenly cover the spores, and the sample was then left to air dry in the biosafety cabinet. After drying, the thin PVA film was stripped off the gold foil and resuspended in sterile DI water. The gold foil was then placed into DI water and sonicated for 30 min at room temperature to remove residual spores. Spores recovered from PVA stripping and sonication steps were combined for further analysis. This method was first tested with untreated control *B. anthracis* spores that were air dried on a gold foil substrate, proving it to be biocompatible (i.e., does not affect spore colony formation ability) and demonstrating 95% or higher recovery efficiency. The recovered spore suspension was then centrifuged at 4,000 rpm for 10 min to separate the spore pellet from the supernatant. Spore pellets were further washed with sterile DI water three more times to remove residue PVA. The supernatant was used for spore constituent leakage studies.

Inactivation assay. Spore pellets from the recovery step were resuspended in sterile DI water, and the number of spores per ml was determined using a hemocytometer. Appropriate dilutions of each sample were then plated on nutrient agar plate incubated overnight at ~35°C. The number of colonies was counted to determine spore colony formation ability.

Nanoscale structural and mechanical analysis by AFM. Nanoscale topographical and mechanical analysis of individual spores was realized by AFM in air. Briefly, a very dilute suspension of recovered spores was placed on freshly cleaved mica substrate and left in the biosafety cabinet to air dry. The AFM cantilever carried a single crystal silicon tip, with a spring constant of 40 N/m and a tip radius of 5 nm. The instrument we use to image the *Bacillus* spores and measure materials properties of the spore surface is a Nanoscope MultiMode atomic force microscope with peak force imaging capability from Bruker Corporation. The atomic force microscope was operated in intermittent-contact mode, in which the AFM tip oscillates with a small amplitude (10 to 100 nm) and at a low modulation frequency (0.5 to 2 kHz). The force of contact was measured at the modulation frequency and used for the force control feedback electronics. The static load was maintained as a small preset value (0.3 to 30 nN). The AFM instrument is equipped with a scanner (AS-130VLR) that is capable of imaging 125 μm by 125 μm in the lateral *x*- and *y*-axis direction and 5 μm in the vertical *z*-axis direction. During a typical peak force imaging process, the instrument acquires and analyzes the individual force curves from each cycle of contact. Surface properties, such as adhesion, modulus, dissipation, and deformation, are simultaneously measured and processed using the commercial MultiMode 8 nanoscope analysis software. The modulation frequency is significantly lower than the cantilever resonant frequency so that there is enough bandwidth for fast data sampling and analysis in real time. The direct force measurement at high speed allows the force distance data to be analyzed directly without ambiguity.

The adhesion force is determined from the pull-off position in the force-distance curve on each point of contact. The adhesion force can be produced by any attractive forces, such as van der Waals force, electrostatics, and capillary meniscus of thin liquid film on the sample surface. The topographic morphology of the surface may affect interfacial adhesion, since the adhesion typically increases with increasing tip size and area of contact. For silicon-based cantilever probes, the surface of the probe is usually covered with hydroxyl groups due to surface reactions with water in air. The adhesion force between the hydrophilic probe and

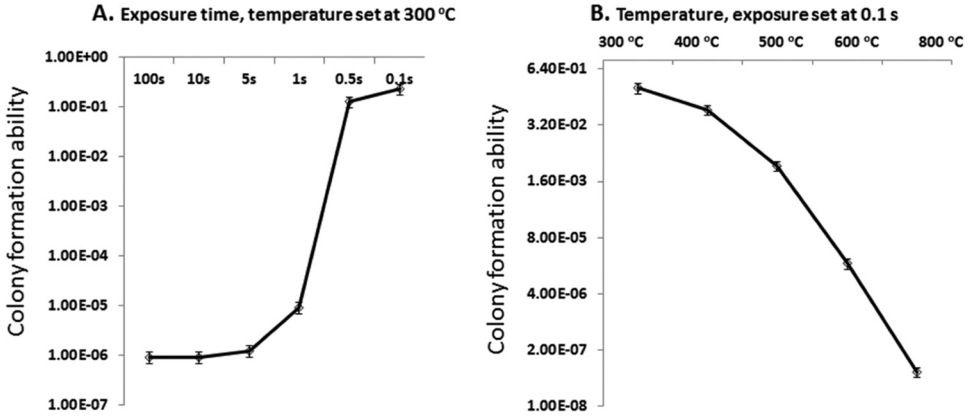

FIG 1 Heating conditions and corresponding spore colony formation ability, defined as the number of colonies formed divided by the number of spores plated. (A) Constant temperature, different exposure times; (B) constant exposure time, different temperatures. Data shown are averages of 6 replicates, and error bars are standard errors.

sample surface is likely dominated by hydrogen bonds in water and other polar molecules on the surface.

The Young's modulus of the sample was obtained by fitting the unloading portion of the force-distance curve using the Derjaguin-Muller-Toporov (DMT) model (44), as given by

$$F - F_{\text{adhesion}} = \frac{4}{3}E^* \sqrt{R(d - d_0)^3}$$

where F is the load, F_{adhesion} is the adhesion force, E^* is the reduced modulus, R is the radius of the tip, and $d - d_0$ is the deformation in the surface. The reduced modulus is defined by

$$E^* = \left(\frac{1 - V_s^2}{E_s} + \frac{1 - V_{\text{tip}}^2}{E_{\text{tip}}} \right)^{-1}$$

where n is the Poisson's ratio, E_{tip} is the Young's modulus of the tip, and E_s is the Young's modulus of the sample.

SEM imaging of inactivated spores. Inactivated spores (as confirmed by the inactivation assay) were placed on an appropriate substrate, air dried, and imaged directly using a vacuum scanning electron microscope (SEM) without sputter coating with metals. For each sample, at least 50 randomly selected spores were imaged and used in measurement.

Assessment of spore inner structure integrity. Two additional experiments were performed to assess the integrity of the spore inner structure by studying (i) the leakage of spore biomolecules (nucleic acids and soluble proteins) from the damaged spores and (ii) accessibility of a nuclear dye (45) to the spore core. For the first purpose, we collected supernatant from suspensions of recovered spores to measure leaked biomolecules. Nucleic acid content was determined by mixing with Syto 16, a dye that shows dramatic increase in fluorescence upon nucleic acid binding. The fluorescence signal was determined by a fluorescence spectrometer (FluoLog 3; HORIBA) (excitation, 480 nm; emission, 520 nm). Soluble spore material in the supernatant was determined by measuring the UV absorbance at 280 nm. In the second experiment, damaged spores were incubated with Syto 16 for 30 min, washed with DI water, and imaged using a fluorescence microscope (filter set; excitation, 488 nm; emission, 520 nm). The rationale for this experiment is based on the fact that Syto 16 cannot penetrate the dormant spore core because of the barrier from the inner membrane (44). Therefore, Syto 16 fluorescence can be used as an indicator of a compromised inner membrane.

Image analysis. Correlation of the different images (height and adhesion force) was achieved by using the NIH Image J software. Syto 16 fluorescence staining was quantified by performing the Image J "Analyzing particles" function on fluorescence microscopy images of the inactivated spores.

RESULTS

Spore inactivation by rapid dry heat. The spore survival probability measured under different heat inactivation conditions is shown in Fig. 1. As expected, for a given temperature (300°C), spore colony formation ability decreased with increasing exposure time (0.1 to 100 s). The relationship, however, is not linear: the largest reduction took place between 0.5 and 1 s, it since became smaller and eventually flattened out after 5 s. The scenario was different when the exposure time was kept constant, and only the temperature was varied for different samples. In this case, the increase in temperature caused a steady decrease in colony formation ability within the tested temperature range (300 to 800°C). Heated spore samples with a colony formation ability of 10^{-6} or less (e.g., 300°C for ≥10 s and 800°C for 0.1 s) were selected for further quantitative nanomechanical analysis using AFM and SEM. This is to ensure that the majority of spores seen under these high-magnification techniques are indeed inactivated spores; thus, the results can be unambiguously attributed to the properties of inactivated spores.

Quantitative nanomechanical analysis of inactivated spores. We first compared the morphological differences between spores from two selected heat treatments: 300°C for 10 s (low temperature, long exposure) and 800°C for 0.1 s (high temperature, short exposure). Figure 2 shows the representative SEM and AFM images of spores inactivated by the respective treatment. Two types of AFM images are shown here, the height images and the peak force error images; peak force error images were provided to show the finer details which cannot be properly visualized in the height images due to the large range of image depth. Images of untreated viable *B. anthracis* spores are included as a control. Height measurements showed that the average heights of these spores are 774 ± 41 nm for the untreated live spores, 671 ± 106 nm for lower-temperature-inactivated spores, and 594 ± 153 nm for the high-temperature-inactivated spores. It is also obvious from these images (Fig. 2A to C) that the surfaces of untreated spores have a rather smooth and plump appearance (with small nanometer-sized clumps visible on the peak force error images), typical for a *B. anthracis* Sterne spore covered by an intact exosporium (35, 36). In contrast, the surfaces of the heat-inactivated spores are

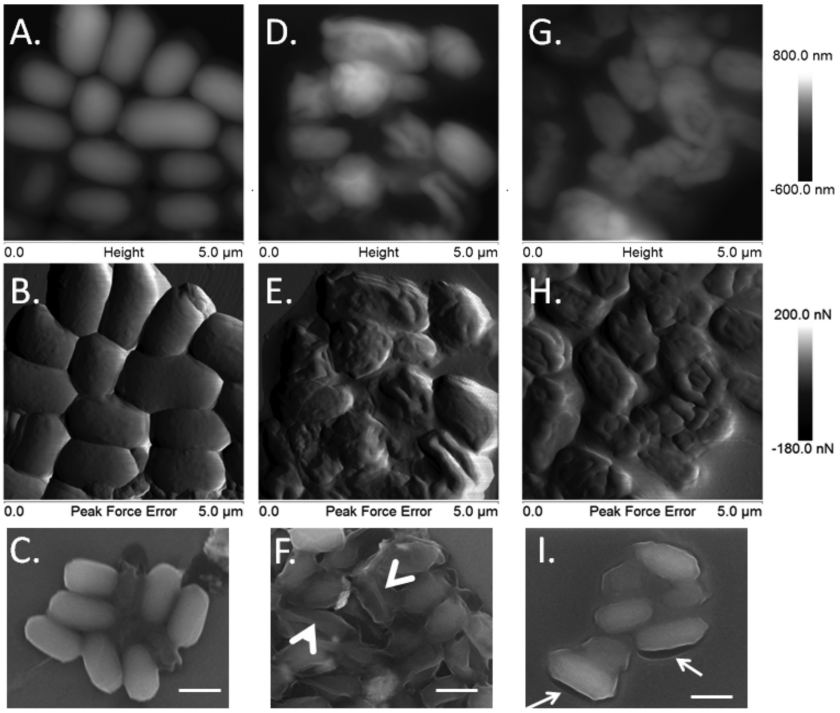

FIG 2 Spore morphology shown as AFM height (A, D, and G), AFM peak force error (B, E, and H), and SEM images (C, F, and I). (A to C) Untreated viable spores; (B to F) spores inactivated at 300°C for 10 s; (G to I) spores inactivated at 800°C for 0.1 s. Note that due to the differences in sample preparation for the two imaging techniques, the specific spore clusters in the AFM images are not the same clusters of spores shown in the SEM images. The white arrowheads indicate folds, and the white arrows indicate the "gap-like" structures. Bars in the SEM images, 1 μm.

rather rough-looking as shown by the AFM images. For the two heat-inactivated groups, spores treated at 300°C for 10 s seemed to have a thin layer of covering. On some spores, folds of this thin layer are clearly visible (indicated by white arrowheads in Fig. 2F). These folds have an average roughness of 157 ± 14.6 nm and are visible in both the AFM and SEM images. Spores inactivated at higher temperature (800°C for 0.1 s) do not have this film layer and are characterized with thick fiber-like structures that are 160 to 190 nm in width and run mostly in the longitudinal direction, occasionally in the lateral direction. The morphology and location of these structures resemble the surface ridges seen in exosporium-less *B. anthracis* spores (35). Figure 3 is a collection of higher-

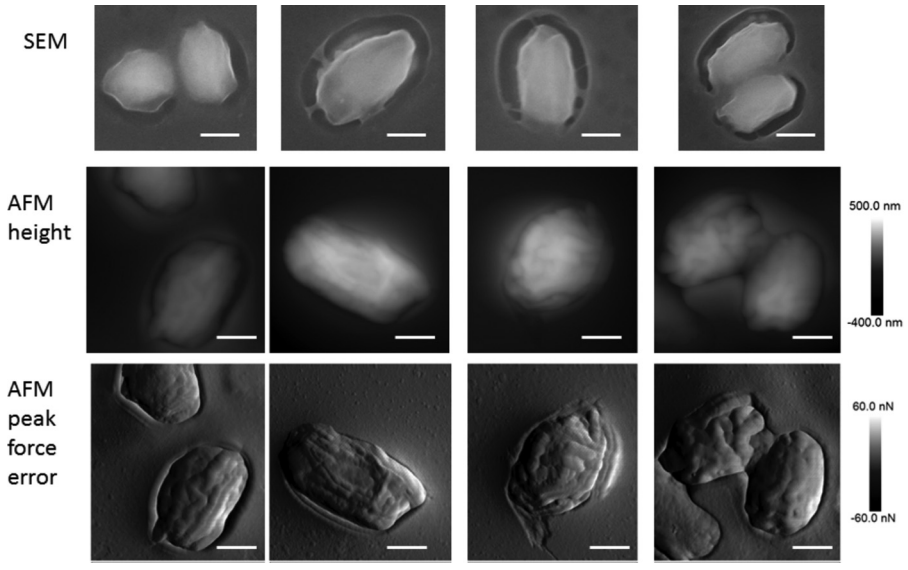

FIG 3 "Gap-like" feature at the edge of some spores inactivated by a high-temperature, short-exposure treatment (800°C for 0.1 s). The "gap-like" structures are most pronounced in the SEM images and visible although not as obvious in AFM height and peak force error images. Note again that the specific spores in the AFM images are not the same individual spores shown in the SEM image. Bars, 500 nm.

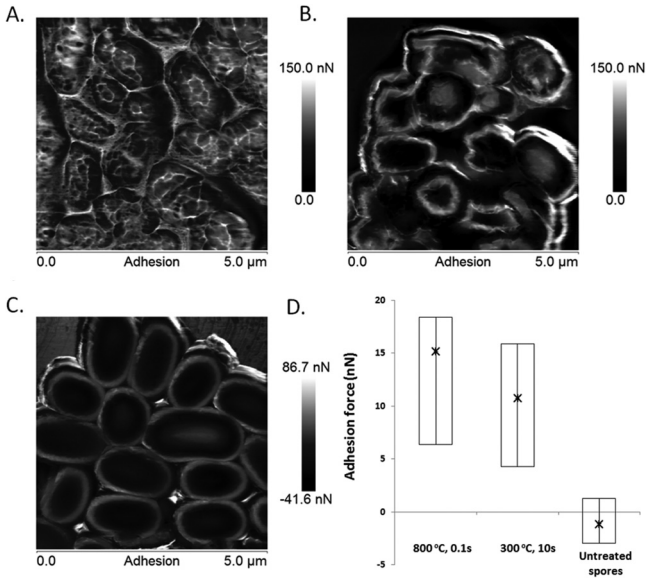

FIG 4 Representative AFM adhesion force images of the spores inactivated by rapid dry heat. (A) High temperature, short exposure (800°C, 0.1 s); (B) low temperature, long exposure (300°C, 10 s); (C) untreated viable spores as a control; (D) graph showing the median adhesion force (indicated by ×); and the 10th to 90th percentile data ranges (the bottom of the boxed area shows the value for the 10th percentile and the top of the boxed area shows the value for the 90th percentile; based on measurements of ~100 randomly selected spores).

resolution images of individual spores, including one that is clearly shown with 2 closely appositioned ridges (AFM height and peak force error images). The surface roughness of these ridges is 34 ± 3.6 nm and not visible in the SEM images, likely due to the lower resolution of SEM in the *z* direction. SEM images of some spores in the higher-temperature treatment group showed a "gap-like" structure at the boundaries (Fig. 3 and the areas indicated by white arrows in Fig. 2I). AFM images showed similar structures at the edges, but with some differences that are likely due to the nature of the two imaging techniques (secondary electron emission in SEM versus force microscopy in AFM).

Nanomechanical analysis of inactivated spores. (i) Adhesion force. Adhesion force reflects the interaction between the AFM cantilever tip and the surface of the sample under study. A higher adhesion force suggests that there was a stronger attractive force between the tip and the very top layer of the spore surface, and negative adhesion force values are suggestive of repulsive forces. Our results clearly showed that inactivated spores by both treatments showed significantly higher adhesion force than the untreated viable spores ($P < 0.0001$ by unpaired *t* test) (Fig. 4). In untreated viable spores, adhesion forces between the unmodified hydrophilic silicon cantilever and spore surface are comparatively small, with a negative average value, suggesting an overall repulsive interaction. This is reasonable since hydrophilic-hydrophobic interactions are major contributors to AFM tip-sample adhesion forces, and intact mature *B. anthracis* spores are known to have hydrophobic surfaces (46, 47) that would repel the hydrophilic AFM tip. On an individual spore level, a difference exists between the center and periphery of the spore surface. Some spores have a "concave-looking" adhesion map (signal in the center lower than the edges), while some have a "convex" appearance. Generally, the variations in adhesion force on control spore surfaces are relatively small compared to those found in the inactivated spores. Between the two heat-inactivated groups, the high-temperature group has a high median adhesion force value, but the 10% to 90% adhesion force ranges are similar, with the values for the high-temperature group slightly higher.

Another obvious observation from Fig. 4 is the difference of adhesion force distribution among the spores. Spores inactivated by high temperature (800°C for 0.1 s) showed a net-like adhesion force pattern. The peaks and valleys of the adhesion force correlate well with the topography of the cable-like structures (Fig. 5A). Although there are small spore-to-spore variations in the adhesion force pattern, most spores exhibited similar appearances. Spores inactivated at lower temperature (300°C for 10 s), however, showed large spore-to-spore variations in their adhesion force distribution (Fig. 5B, C, and D). Most times, the adhesion force does not closely correlate with topography. Even spores with similar topography (note the two spores indicated by white arrows in Fig. 5B) can have drastically different force distribution: some resemble the untreated spores, with a "concave-looking" adhesion map (signal in the center lower than the edges), while others show a "convex-looking" adhesion map (signals in the center higher than the edges). The peak and valley differences are 30 to 50 nN and 60 to 80 nN for the high-temperature and low-temperature treatment, respectively.

Because adhesion force is a measure of the interactions of spore surface chemical groups and the AFM silicon cantilever, changes in adhesion force magnitude and distribution can be viewed as an indicator of the alterations and reorganization of surface chemical groups. Untreated viable spores uniformly showed an overall repulsive interaction with the hydrophilic AFM tip, likely a result of the hydrophobic proteins on the exosporium (2). Heat-inactivated spores showed much higher adhesion force, suggesting the removal or reorganization of these hydrophobic domains on the surface. The removal of the top surface layer (exosporium layer or even some coat) will lead to the exposure of underlying structures that are less hydrophobic, such as the peptidoglycan-rich cortex (46), thus resulting in stronger adhesion to the cantilever. Spores inactivated at a lower temperature were quite different: although the overall average adhesion force was significantly higher than for untreated control spores, the large spore-to-spore variation indicates a more complicated process. The presence of a thin film layer suggests at least partial retention of the exosporium or the outer coat. In some cases, this layer remained attached to the spore on all sides. In this situation, dehydration and heat-induced protein denaturation and reaction might account for the increases in adhesion force. In other cases, this layer was only partially attached to the spores at a few sites on one side and subjected to flipping over (with the attachment sites serving as hinges) during sample recovery and preparation for imaging. Therefore, the observed changes in adhesion force could be the exposure of the biomolecules on the inner side of this thin layer and uncovering of the underlying spore structures.

(ii) Young's modulus. Modulus is a measure of elastic stiffness of the material under study. In this case, we have discovered that spores inactivated by rapid heat treatment are significantly (*P* value < 0.0001 by unpaired *t* test) stiffer than untreated viable spores (Fig. 6D). However, there is no significant difference in spore stiffness between the two heating conditions (*P* value > 0.1). The observed increase in stiffness after heat inactivation might be

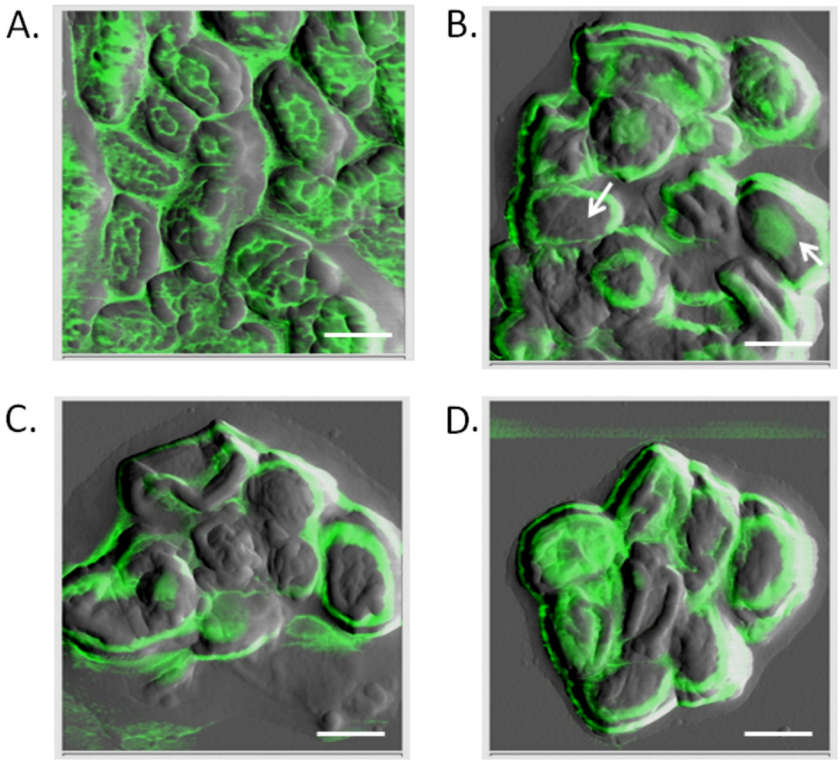

FIG 5 Overlay of AFM peak force error (gray) and adhesion force (green) images. (A) High temperature, short exposure (800°C, 0.1 s); (B, C, and D) three different spore clusters inactivated under low-temperature, long-time exposure (300°C for 10 s). The white arrows in panel B indicate two spores with similar topographies but different adhesion force patterns. Bars, 1 μm.

the result of one (or the combination) of the following factors: (i) change in water content in the spore, which has been shown to affect measurement of modulus in spores (36) and isolated bacteria peptidoglycan (major component of the spore cortex) (48); and/or (ii) heat-induced denaturation and aggregation of spore biomolecules that result in hardening of the spore.

In order to confirm that the differences we observed were indeed related to heating temperature, not due to some postmortem effects, we imaged spores heated at the intermediate temperature of 500°C for 0.1 s (Fig. 7). AFM images of spores heated at 300°C for 0.1 s were included as a comparison. The most striking difference between these two temperatures, as shown in Fig. 7, is the difference in the adhesion force image. Spores heated at 300°C for 0.1 s showed an adhesion force map similar to that of the untreated viable spores (Fig. 4C). In contrast, many spores heated at 500°C showed a bright line (indicating stronger attraction force) along the longitudinal middle line (Fig. 7C), while some showed cable-like structures (indicated by a white arrow in Fig. 7C), as seen in spores treated at 800°C (Fig. 4A). Some of these bright lines are accompanied with a bright knob of about 200 to 300 nm in diameter. These bright lines/spots on an otherwise hydrophobic surface probably resulted from heat-induced cracking of the superficial hydrophobic layer, exposing the more hydrophilic layers underneath. This cracking phenomenon is probably the initiating event that led to the removal of the superficial layer as seen in the 800°C case.

Effects of continued heating beyond inactivation. In order to understand the effects of long-time exposures on spore inactivation efficiency, we increased the exposure time at 300°C. Our results showed that increasing the exposure time to 100 s resulted in only a small increase in inactivation efficiency but produced significant changes in spore morphology. Spores heated under prolonged exposure appeared strikingly different from spores from any other aforementioned treatments. These spores took on a coffee bean-like morphology with a "groove" at the center line (Fig. 8). The average height of the remaining spores at 449 ± 23 nm is much smaller, and the depth of the groove is about 131 ± 14 nm. This is a significant reduction from 670 nm, which is the average height of spores inactivated under the same temperature but for a shorter time (300°C for 10 s). This reduction indicates significant loss of spore materials. The first important observation is the smoothness of the surface of the remaining spore structure, which shows no apparent surface ridges or rodlets that are characteristic of spore outer and inner coats (25, 27, 29, 35, 49). Moreover, the adhesion force image showed a rather uniform adhesion force on the spore surface, unlike spores inactivated under the other two heating conditions, suggesting a chemically different material. On the basis of these observations, we speculate that these spores had probably lost most of their outer layers, and the remaining structures were likely the core or spore body, which had been shown to have a relatively smooth appearance (50). It is difficult to tell whether the inner membrane is still retained. Another important observation from these AFM images is formation of the "groove" at the center line along the longitudinal direction. We suspect that this might be the result of either collapsed spore cores (due to the loss of volatile spore core components) or burst spore cores (due to internal pressure buildup). The collapsed structures of the spores indicated that the structural damage may be caused by

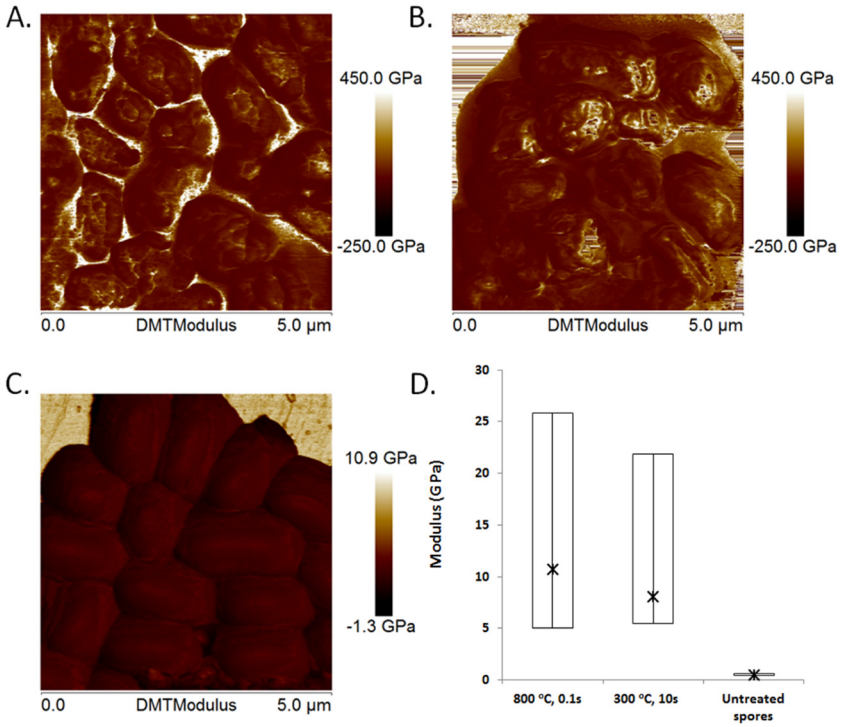

FIG 6 Young's moduli of the heat-inactivated spores. (A) Spores heated at 800°C for 0.1 s; (B) spores heated at 300°C for 10 s; (C) untreated viable spores; (D) graph showing the median modulus (indicated by ×) and the 10th to 90th percentile data ranges (the bottom of the boxed area shows the value for the 10th percentile and the top of the boxed area shows the value for the 90th percentile; based on measurements of ~100 randomly selected spores). DMTModulus, Derjaguin-Muller-Toporov modulus.

thermal mechanical stress that is concentrated in the longitudinal direction, because the mechanical strength along the structural cables is expected to be stronger than that perpendicular to these cables.

Spore inner structure integrity assessment. (i) Syto 16 nucleic acid staining of *B. anthracis* spores. Syto 16 is a nuclear dye that is able to diffuse through the cell plasma membrane and is therefore a popular dye for live-cell staining. It cannot penetrate into a dormant spore core, but it is able to enter the core of fully germinated spores, bind nucleic acids, and exhibit strong green fluorescence (51, 52). This difference has been attributed to the structural barrier of the inner membrane (45). Quantitative mea-

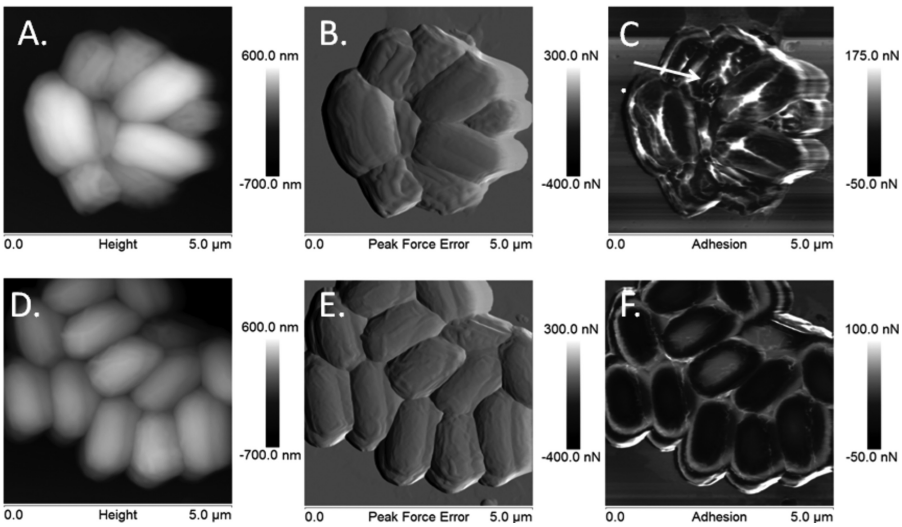

FIG 7 (A to C) Typical AFM images of spores heated at an intermediate temperature (500°C). (D to F) Images of spores treated at 300°C for 0.1 s were included for comparison. Note the striking difference in the adhesion force map: while the distribution pattern for spores in the 300°C group was similar to that for untreated viable spores (Fig. 4C), the 500°C image has a bright line along the longitudinal central line, and some spores (indicated by a white arrow) showed cable structures similar to the ones observed in spores treated at 800°C (Fig. 4A). Images have been individually scaled to yield the best visual effect.

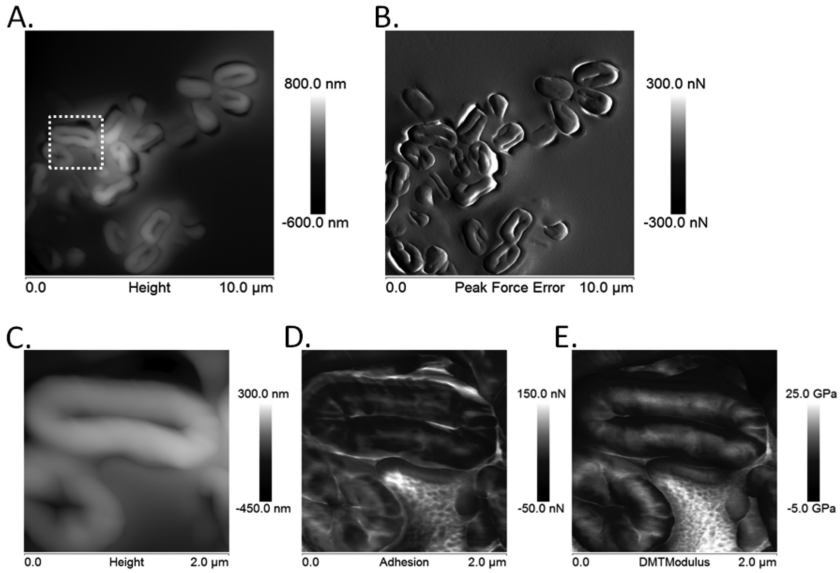

FIG 8 Spores heated for 100 s at 300°C. (A) AFM height image; (B) AFM peak force error image; (C, D, and E) high-resolution height, adhesion force, and modulus images of two representative spores within the box outlined by a white dotted line in panel A.

surements of the fluorescence intensity of representative spores showed higher fluorescence signals for the group treated at a high temperature compared to the group treated at a lower temperature (Fig. 9A). The fluorescence intensities for both of these groups are significantly higher than that for the untreated viable spores, indicating increased permeability of the inner membrane to Syto 16. It is worth noting that significant variability in stain intensity occurs among inactivated spores in the same treatment group, suggesting the inner membrane damage in these inactivated spores is not uniform.

(ii) Leakage of spore constituents. As shown in Fig. 9B, nucleic acid release from the spores inactivated by lower-temperature treatment (300°C for 10 s) was almost at the baseline level. Nucleic acid release from the 800°C-treated spores is significantly higher, above the baseline. However, the total amount of leaked nucleic acid even in the spores treated at high temperature is small as shown by the weak fluorescence signal (Syto 16 fluorescence when it complexes with leaked nucleic acids in the supernatant). This suggests that although there is structural damage, the damage to the inner membrane is not so severe to remove most of the nucleic acid material from inside the spore. In contrast, UV 280 absorbance in both cases was significantly higher than the baseline level (Fig. 9C). Therefore, there is significant leakage of other spore constituents (e.g., coat proteins and dipicolinic acid [DPA]) in both cases. Future analysis (high-performance liquid chromatography [HPLC] and mass spectrometry analysis) of the composition of the leaked molecules will provide more insights on the sources of the leaked protein components.

DISCUSSION

Rapid dry-heat inactivation. Compared with common laboratory dry heating studies, temperatures in this study are much higher (from 300°C to 800°C as opposed to 120°C), and the exposure times are significantly shorter (0.1 to 10 s versus 30 to 120 min

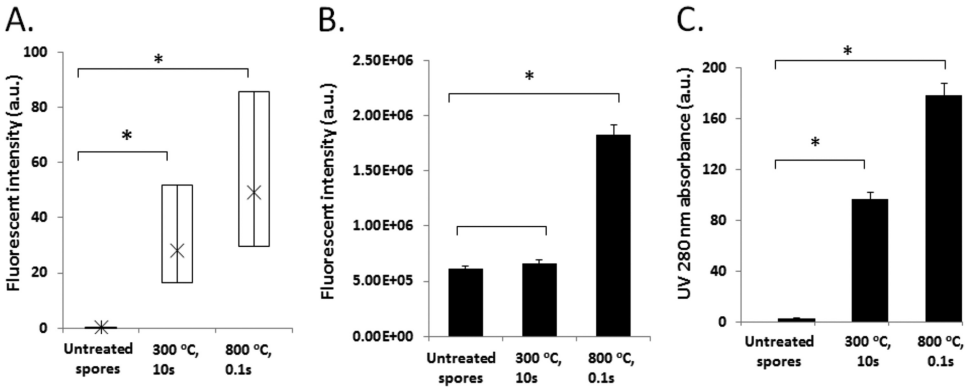

FIG 9 Spore inner structure integrity assessed by three different methods. (A) Nucleic acid staining in spores (shown as the median [×] and 10th to 90th percentile [box] fluorescence intensity of Syto 16-stained spores; based on measurements of 100 randomly selected spores). (B and C) Nucleic acid leakage (B) and leakage of soluble spore components as measured by UV 280 absorbance (C). Data in panels B and C are averages of 6 replicates, and error bars are standard errors. All graphs are shown in arbitrary units (a.u.). Values that are significantly different ($P < 0.01$) are indicated by a bar and asterisk.

[6]). This type of high-temperature rapid heating is found in military situations or environmental decontamination with a high-temperature plume. It has been suggested that the killing mechanism under rapid high-temperature heating might differ from long-term, low-temperature heating conditions (8, 20). This is reasonable since at very short timescales (less than 1 s), the timescales of processes such as heat and mass transfer in a spore become comparable to heating times and may contribute significantly to spore killing in addition to that from heat-promoted biochemical reactions. By far, only a very limited number of studies have addressed this issue, so the inactivation mechanism under short-time heating conditions is just being unraveled (19, 20, 53). One recent finding is that mutational damage is involved in the causal chain of events leading to inactivation of aerosolized endospores exposed to heat for subsecond time periods (19). In this study, we attempted to provide insights in spore inactivation from the perspective of structural damages by using atomic force microscopy and other techniques.

Nanoscale analysis shed new insights on the heat inactivation mechanism. Our results (especially AFM results) have shown completely different surface topography patterns, adhesion force maps, and elastic properties (modulus) for spores inactivated rapidly by dry heat. Inactivated spores lost the plump look of native untreated spores, likely due to the loss of intraspore water and the rupture of outer spore layers. Spores inactivated at a lower temperature (300°C) for a longer time (10 s) appeared to retain a thin layer of covering, which could be the exosporium or outer coat. Attached and folded coat appear frequently, and occasionally, there is a dislocated coat from the spore (data not shown). It appears that at 300°C, the spores went through a dehydration process: intraspore water molecules vaporize and escape from the spores, leaving a shriveled-looking spore behind. It has been shown several times that the bacterial spore coats are able to fold and unfold as a response to changes in the humidity (25). In the current study, the loss of water appears to be irreversible since the spores did not return to the plump-looking appearance even after rehydration in water. Prolonged heating for 100 s resulted in further structural damage with the loss of more outer layers, probably including the cortex, leaving a smooth concaved, coffee bean-like structure behind. The coffee bean-like-structure could be the result of a collapsed inner core structure. In the spores inactivated by high temperature (800°C for 0.1 s), we have observed the absence of the superficial thin layer that is found in the spores treated by lower temperature (300°C for 10 s).

We believe that the above observations are associated with the thermal and mechanical stresses built up within the spore upon rapid heating. According to previous modeling studies (36, 57), heat transfer within a spore is very rapid: it requires less than 1 ms (for well-dispersed, isolated spores) to 21 ms (for spores in a 1,000-spore cluster) for a spore to reach the steady-state temperature. As the spore core temperature rises rapidly, its water content (both chemically bonded and mobile water molecules) starts to vaporize and expand. If the vaporized content cannot diffuse out of the spore in time, pressure will build up inside the spore. Mechanical stresses caused by the buildup of pressure, once exceeding a stress-rupture limit, will cause the spore to fail structurally (likely first along the longitudinal direction as shown in Fig. 7). Another possible source of the thermal stress buildup is due to differential thermal expansion between different layers of the spore structures. Spores experiencing the 0.1-s 800°C heating condition will have distinctly greater thermal and mechanical stresses gradients across the spore structure than spores experiencing the 10-s 300°C treatment. The differences in surface topography and nanomechanical properties are probably direct results of this differential thermal and mechanical loading. Current results do not provide sufficient insights into damage to the inner layers of the spore structures and the critical biochemical events that led to eventual spore inactivation. However, it is very probable that these spores inactivated under two heating conditions differ in these two aspects as well.

AFM nanomechanical analysis of biological samples in air versus in fluid. The nanomechanical analysis in this study was carried out in ambient air, and we are aware that this is not the ideal condition for nanomechanical analysis. Ideally, nanomechanical analysis of biological samples should be performed in a fluid environment for the reason that most cells, unlike spores, require sufficient hydration to stay alive, and also conducting the experiment in liquid circumvents the issue of the capillary meniscus effect in air (54–56). The latter is extremely important for molecular recognition studies in which the focus is the molecular interactions between molecules. In the current study, all of the nanomechanical analysis was performed under ambient lab conditions; therefore, the values (adhesion force and Young's modulus) obtained are expected to differ from those obtained in aqueous environments. For instance, the Young's moduli of spores measured in a fluid environment are of much smaller magnitude than the values in this study (38). However, AFM in air is a much easier and less time-consuming experiment involving less-stringent sample preparation, as it is well-known that it is not a trivial task to keep spores attached to and immobilized on a substrate in a liquid environment (30, 33). Besides, our goal for this study is not to accurately determine the actual nanomechanical properties of the spores. Instead, we intend to use it as a rapid, direct comparative tool to differentiate spores inactivated under various heating conditions. In this respect, it has proved very useful by quickly revealing the remarkable differences among the various spore preparations in this study: the untreated viable spores, the high-temperature-inactivated spores and the low-temperature-inactivated spores. These direct, visual differences point to likely different inactivation mechanisms without sophisticated biochemical assays.

Previous biochemical and molecular biological studies suggested that dry heat inactivates bacterial spores mainly through DNA damage as evidenced by the high-frequency mutations in dry-heat survivors as well as the abundance of single-strand breaks in DNA isolated from dry-heat-treated spores. This damage process is hindered by the presence of the small acid soluble proteins, which also protect spores from other types of stresses (wet heat, oxidizing agents, and desiccation) (4, 14). Given the differences in structural damage caused by the two temperature regimes in this study, it will be worthwhile to find out, as we anticipate, if there are differences in biochemical and molecular biological effects in these differently inactivated spores. Future work therefore will include the quantitative identification and mapping of DNA damage using molecular biology and mass spectrometry techniques.

Conclusion. In this work, we developed and applied a heat treatment method that is capable of heating spores in a rapid thermal treatment with accurately controlled temperature and exposure time. Using AFM, we performed nanoscale analysis on the heat-inactivated spores under different temperature/time combi-

nations. Our results showed drastically different morphology and surface nanomechanical properties in spores inactivated under different heating conditions. We attributed these differences to the differential thermal and mechanical stresses inside rapidly heated spores. The effects of buildup of internal thermal and mechanical stresses become more prominent in ultrafast, high-temperature heat inactivation, when the heat-induced vapor generation and differential thermal expansions inside the spore far exceed the yield strength of the spore. It remains to be determined whether there is a correlation between the structural/nanomechanical changes and the biochemical changes that are directly linked with spore inactivation. In summary, this study has provided novel insights into inactivation of *Bacillus anthracis* spores by rapid heating by the evaluation of structural damage and changes in nanomechanical properties. The findings in this study suggest that AFM in ambient laboratory conditions can be used to quickly distinguish spores that were thermally inactivated (e.g., viable spores versus heat-inactivated spores) and also distinguish spores that were inactivated by very high-temperature, short-time exposures from those inactivated by low-temperature, long-time thermal treatments.

ACKNOWLEDGMENTS

This work was supported in part by the Defense Threat Reduction Agency through a program managed by Suhithi Peiris.

The views expressed in this paper are those of the authors and do not reflect the official policy or position of the United States Air Force, the Department of Defense, or the United States government.

REFERENCES

1. **Driks A.** 2002. Overview: development in bacteria: spore formation in Bacillus subtilis. Cell. Mol. Life Sci. **59:**389–391. http://dx.doi.org/10.1007/s00018-002-8430-x.
2. **Henriques AO, Moran CP, Jr.** 2007. Structure, assembly, and function of the spore surface layers. Annu. Rev. Microbiol. **61:**555–588. http://dx.doi.org/10.1146/annurev.micro.61.080706.093224.
3. **Piggot PJ, Hilbert DW.** 2004. Sporulation of Bacillus subtilis. Curr. Opin. Microbiol. **7:**579–586. http://dx.doi.org/10.1016/j.mib.2004.10.001.
4. **Setlow P.** 2006. Spores of Bacillus subtilis: their resistance to and killing by radiation, heat and chemicals. J. Appl. Microbiol. **101:**514–525. http://dx.doi.org/10.1111/j.1365-2672.2005.02736.x.
5. **Tufts JA, Rosati JA.** 2012. Thermal inactivation of Bacillus anthracis surrogate spores in a bench-scale enclosed landfill gas flare. J. Air Waste Manag. Assoc. **62:**151–159. http://dx.doi.org/10.1080/10473289.2011.636862.
6. **Spotts Whitney EA, Beatty ME, Taylor TH, Jr, Weyant R, Sobel J, Arduino MJ, Ashford DA.** 2003. Inactivation of Bacillus anthracis spores. Emerg. Infect. Dis. **9:**623–627. http://dx.doi.org/10.3201/eid0906.020377.
7. **Popham DL, Sengupta S, Setlow P.** 1995. Heat, hydrogen peroxide, and UV resistance of Bacillus subtilis spores with increased core water content and with or without major DNA-binding proteins. Appl. Environ. Microbiol. **61:**3633–3638.
8. **Grinshpun SA, Adhikari A, Yermakov M, Reponen T, Dreizin E, Schoenitz M, Hoffmann V, Zhang S.** 2012. Inactivation of aerosolized Bacillus atrophaeus (BG) endospores and MS2 viruses by combustion of reactive materials. Environ. Sci. Technol. **46:**7334–7341. http://dx.doi.org/10.1021/es300537f.
9. **Coleman WH, Zhang P, Li YQ, Setlow P.** 2010. Mechanism of killing of spores of Bacillus cereus and Bacillus megaterium by wet heat. Lett. Appl. Microbiol. **50:**507–514. http://dx.doi.org/10.1111/j.1472-765X.2010.02827.x.
10. **Tabit FT, Buys E.** 2010. The effects of wet heat treatment on the structural and chemical components of Bacillus sporothermodurans spores. Int. J. Food Microbiol. **140:**207–213. http://dx.doi.org/10.1016/j.ijfoodmicro.2010.03.033.
11. **Setlow B, Setlow P.** 1998. Heat killing of Bacillus subtilis spores in water is not due to oxidative damage. Appl. Environ. Microbiol. **64:**4109–4112.
12. **Damit B, Lee C, Wu CY.** 2011. Flash infrared radiation disinfection of fibrous filters contaminated with bioaerosols. J. Appl. Microbiol. **110:**1074–1084. http://dx.doi.org/10.1111/j.1365-2672.2011.04965.x.
13. **Molin G, Ostilund K.** 1975. Dry-heat inactivation of Bacillus subtilis spores by means of infra-red heating. Antonie Van Leeuwenhoek **41:**329–335. http://dx.doi.org/10.1007/BF02565067.
14. **Setlow B, Setlow P.** 1995. Small, acid-soluble proteins bound to DNA protect Bacillus subtilis spores from killing by dry heat. Appl. Environ. Microbiol. **61:**2787–2790.
15. **Brannen JP, Garst DM.** 1972. Dry heat inactivation of Bacillus subtilis var. niger spores as a function of relative humidity. Appl. Microbiol. **23:**1125–1130.
16. **Drummond DW, Pflug IJ.** 1970. Dry-heat destruction of Bacillus subtilis spores on surfaces: effect of humidity in an open system. Appl. Microbiol. **20:**805–809.
17. **Alderton G, Snell N.** 1969. Chemical states of bacterial spores: dry-heat resistance. Appl. Microbiol. **17:**745–749.
18. **Angelotti R, Maryanski JH, Butler TF, Peeler JT, Campbell JE.** 1968. Influence of spore moisture content on the dry-heat resistance of Bacillus subtilis var. niger. Appl. Microbiol. **16:**735–745.
19. **Johansson E, Adhikari A, Reponen T, Yermakov M, Grinshpun GA.** 2011. Association between increased DNA mutational frequency and thermal inactivation of aerosolized Bacillus spores exposed to dry heat. Aerosol Sci. Technol. **45:**376–381. http://dx.doi.org/10.1080/02786826.2010.538452.
20. **Grinshpun SA, Adhikari A, Li C, Reponen T, Yermakov M, Schoenitz M, Dreizin E, Trunov M, Mohan S.** 2010. Thermal inactivation of airborne viable Bacillus subtilis spores by short-term exposure in axially heated airflow. J. Aerosol Sci. **41:**352–363. http://dx.doi.org/10.1016/j.jaerosci.2010.01.007.
21. **Zhang P, Setlow P, Li Y.** 2009. Characterization of single heat-activated Bacillus spores using laser tweezers Raman spectroscopy. Opt. Express **17:**16480–16491. http://dx.doi.org/10.1364/OE.17.016480.
22. **Greer S, Zamenhof S.** 1962. Studies on depurination of DNA by heat. J. Mol. Biol. **4:**123–141. http://dx.doi.org/10.1016/S0022-2836(62)80046-1.
23. **Northrop J, Slepecky RA.** 1967. Sporulation mutations induced by heat in Bacillus subtilis. Science **155:**838–839. http://dx.doi.org/10.1126/science.155.3764.838.
24. **McKenney PT, Driks A, Eichenberger P.** 2013. The Bacillus subtilis endospore: assembly and functions of the multilayered coat. Nat. Rev. Microbiol. **11:**33–44.
25. **Plomp M, Leighton T, Wheeler K, Malkin A.** 2005. The high-resolution architecture and structural dynamics of Bacillus spores. Biophys. J. **88:**603–608. http://dx.doi.org/10.1529/biophysj.104.049312.
26. **Plomp M, Leighton TJ, Wheeler KE, Hill HD, Malkin AJ.** 2007. In vitro high-resolution structural dynamics of single germinating bacterial spores. Proc. Natl. Acad. Sci. U. S. A. **104:**9644–9649. http://dx.doi.org/10.1073/pnas.0610626104.
27. **Plomp M, Leighton TJ, Wheeler KE, Malkin AJ.** 2005. Architecture and high-resolution structure of Bacillus thuringiensis and Bacillus cereus spore coat surfaces. Langmuir **21:**7892–7898. http://dx.doi.org/10.1021/la050412r.
28. **Plomp M, Leighton TJ, Wheeler KE, Pitesky ME, Malkin AJ.** 2005. Bacillus atrophaeus outer spore coat assembly and ultrastructure. Langmuir **21:**10710–10716. http://dx.doi.org/10.1021/la0517437.
29. **Ghosh S, Setlow B, Wahome PG, Cowan A, Plomp M, Malkin A, Setlow P.** 2008. Characterization of spores of Bacillus subtilis that lack most coat layers. J. Bacteriol. **190:**6741–6748. http://dx.doi.org/10.1128/JB.00896-08.
30. **Dupres V, Alsteens D, Andre G, Dufrene YF.** 2010. Microbial nanoscopy: a closer look at microbial cell surfaces. Trends Microbiol. **18:**397–405. http://dx.doi.org/10.1016/j.tim.2010.06.004.
31. **Alsteens D, Dague E, Verbelen C, Andre G, Dupres V, Dufrene YF.** 2009. Nanoscale imaging of microbial pathogens using atomic force microscopy. Wiley Interdiscip. Rev. Nanomed. Nanobiotechnol. **1:**168–180. http://dx.doi.org/10.1002/wnan.18.
32. **Dupres V, Menozzi FD, Locht C, Clare BH, Abbott NL, Cuenot S, Bompard C, Raze D, Dufrene YF.** 2005. Nanoscale mapping and functional analysis of individual adhesins on living bacteria. Nat. Methods **2:**515–520. http://dx.doi.org/10.1038/nmeth769.
33. **Dufrene YF.** 2008. Towards nanomicrobiology using atomic force microscopy. Nat. Rev. Microbiol. **6:**674–680. http://dx.doi.org/10.1038/nrmicro1948.
34. **Muller DJ, Helenius J, Alsteens D, Dufrene YF.** 2009. Force probing

surfaces of living cells to molecular resolution. Nat. Chem. Biol. **5:**383–390. http://dx.doi.org/10.1038/nchembio.181.
35. **Chada VG, Sanstad EA, Wang R, Driks A.** 2003. Morphogenesis of Bacillus spore surfaces. J. Bacteriol. **185:**6255–6261. http://dx.doi.org/10.1128/JB.185.21.6255-6261.2003.
36. **Li A, Xing Y, Burggraf L.** 2013. Thermal effects on surface structures and properties of Bacillus anthracis spores at nanometer scales. Langmuir **29:**8343–8354. http://dx.doi.org/10.1021/la400992q.
37. **Zolock RA, Li G, Bleckmann C, Burggraf L, Fuller DC.** 2006. Atomic force microscopy of Bacillus spore surface morphology. Micron **37:**363–369. http://dx.doi.org/10.1016/j.micron.2005.11.006.
38. **Pinzón-Arango PA, Nagarajan R, Camesano TA.** 2010. Effects of L-alanine and inosine germinants on the elasticity of Bacillus anthracis spores. Langmuir **26:**6535–6541. http://dx.doi.org/10.1021/la904071y.
39. **Pinzón-Arango PA, Scholl G, Nagarajan R, Mello CM, Camesano TA.** 2009. Atomic force microscopy study of germination and killing of Bacillus atrophaeus spores. J. Mol. Recognit. **22:**373–379. http://dx.doi.org/10.1002/jmr.945.
40. **Muller DJ, Dufrene YF.** 2011. Atomic force microscopy: a nanoscopic window on the cell surface. Trends Cell Biol. **21:**461–469. http://dx.doi.org/10.1016/j.tcb.2011.04.008.
41. **Muller DJ, Dufrene YF.** 2008. Atomic force microscopy as a multifunctional molecular toolbox in nanobiotechnology. Nat. Nanotechnol. **3:**261–269. http://dx.doi.org/10.1038/nnano.2008.100.
42. **Nakanishi K, Kogure A, Fujii T, Kokawa R, Deuchi K.** 2012. Development of method for evaluating cell hardness and correlation between bacterial spore hardness and durability. J. Nanobiotechnol. **10:**22. http://dx.doi.org/10.1186/1477-3155-10-22.
43. **Moeller R, Reitz G, Berger T, Okayasu R, Nicholson WL, Horneck G.** 2010. Astrobiological aspects of the mutagenesis of cosmic radiation on bacterial spores. Astrobiology **10:**509–521. http://dx.doi.org/10.1089/ast.2009.0429.
44. **Maugis D (ed).** 2000. Contact, adhesion and rupture of elastic solids. Springer-Verlag, Berlin, Germany.
45. **Kong L, Zhang P, Wang G, Yu J, Setlow P, Li YQ.** 2011. Characterization of bacterial spore germination using phase-contrast and fluorescence microscopy, Raman spectroscopy and optical tweezers. Nat. Protoc. **6:**625–639. http://dx.doi.org/10.1038/nprot.2011.307.
46. **Wiencek KM, Klapes NA, Foegeding PM.** 1990. Hydrophobicity of Bacillus and Clostridium spores. Appl. Environ. Microbiol. **56:**2600–2605.
47. **Doyle RJ, Nedjat-Haiem F, Singh JS.** 1984. Hydrophobic characteristics of *Bacillus* spores. Curr. Microbiol. **10:**329–332.
48. **Thwaites J, Mendelson N.** 1989. Mechanical properties of peptidoglycan as determined from bacterial thread. Int. J. Biol. Macromol. **11:**201–206. http://dx.doi.org/10.1016/0141-8130(89)90069-X.
49. **Carroll AM, Plomp M, Malkin AJ, Setlow P.** 2008. Protozoal digestion of coat-defective Bacillus subtilis spores produces "rinds" composed of insoluble coat protein. Appl. Environ. Microbiol. **74:**5875–5881. http://dx.doi.org/10.1128/AEM.01228-08.
50. **Holt SC, Leadbetter ER.** 1969. Comparative ultrastructure of selected aerobic spore-forming bacteria: a freeze-etching study. Bacteriol. Rev. **33:**346–378.
51. **Black EP, Wei J, Atluri S, Cortezzo DE, Koziol-Dube K, Hoover DG, Setlow P.** 2007. Analysis of factors influencing the rate of germination of spores of Bacillus subtilis by very high pressure. J. Appl. Microbiol. **102:**65–76. http://dx.doi.org/10.1111/j.1365-2672.2006.03062.x.
52. **Black EP, Koziol-Dube K, Guan D, Wei J, Setlow B, Cortezzo DE, Hoover DG, Setlow P.** 2005. Factors influencing germination of Bacillus subtilis spores via activation of nutrient receptors by high pressure. Appl. Environ. Microbiol. **71:**5879–5887. http://dx.doi.org/10.1128/AEM.71.10.5879-5887.2005.
53. **Jung JH, Lee EL, Kim SS.** 2009. Thermal effects on bacterial bioaerosols in continuous air flow. Sci. Total. Environ. **407:**4723–4730. http://dx.doi.org/10.1016/j.scitotenv.2009.05.008.
54. **Xu X, Li J, Li Q, Huang J, Dong Y, Hong Y, Yan J, Qin J, Li Z, Tang BZ.** 2012. A strategy for dramatically enhancing the selectivity of molecules showing aggregation-induced emission towards biomacromolecules with the aid of graphene oxide. Chemistry **18:**7278–7286. http://dx.doi.org/10.1002/chem.201103638.
55. **Xu L, Lio A, Hu J, Ogletree DF, Salmeron M.** 1998. Wetting and capillary phenomena of water on mica. J. Phys. Chem. B **102:**540–548. http://dx.doi.org/10.1021/jp972289l.
56. **Bowen WR, Lovitt RW, Wright CJ.** 2000. Direct quantification of Aspergillus niger spore adhesion in liquid using an atomic force microscope. J. Colloid Interface Sci. **228:**428–433. http://dx.doi.org/10.1006/jcis.2000.6969.
57. **Kumar R, Saurav S, Titov EV, Levin DA, Long RF, Neely WC, Setlow P.** 2011. Thermo-structural studies of spores subjected to high temperature gas environments. Int. J. Heat Mass Transfer **54:**755–765. http://dx.doi.org/10.1016/j.ijheatmasstransfer.2010.11.004.